IEEE Access
Multidisciplinary ⋮ Rapid Review ⋮ Open Access Journal

Received 14 July 2023, accepted 3 August 2023, date of publication 9 August 2023, date of current version 24 August 2023.

Digital Object Identifier 10.1109/ACCESS.2023.3303536

RESEARCH ARTICLE

Harmonic Transponder Sensor Based on Independent Impedance Control for Motion Sensing

JISU KIM, (Student Member, IEEE), SOOYOUNG OH, (Student Member, IEEE), BITCHAN KIM, (Student Member, IEEE), AND JUNTAEK OH, (Member, IEEE)
School of Electronic Engineering, Soongsil University, Seoul 06978, Republic of Korea

Corresponding author: Juntaek Oh (kingojt@ssu.ac.kr)

This work was supported by the National Research Foundation of Korea (NRF) through the Basic Science Research Program under Grant NRF-2022R1F1A1072302.

ABSTRACT This paper presents the design and demonstration of a novel harmonic transponder sensor (HTS) that can measure the position and motion of a target in noisy and reflective indoor environments. In conventional HTS implementation, an impedance mismatch at the input or output can occur because of the impedance variation of the input or output antenna caused by the sensor location or surrounding environment. The impedance mismatch of the input (or output) also affects the output (or input), thereby degrading the conversion gain (CG) of the HTS. An independent impedance control matching network (IICMN) is proposed to deal with the input and output impedances of the HTS separately, regardless of source and load impedance changes. The proposed HTS with an IICMN has a high CG with wide input power and frequency ranges. The proposed HTS was implemented with a size of 44.3-mm × 29.4-mm, and an experiment was conducted to demonstrate its CG. It achieved a peak CG of −14.3-dB at 3.1-GHz. The measured CG remained above −20-dB within a power range of −25-5-dBm at 3.1-GHz and a frequency range of 3.05–3.2-GHz at an input power of −13.7-dBm. The nonlinear responses of the HTS with the dual-band antenna were observed based on the distance and output power. The measurement results showed that the second harmonic signal could be detected at a distance of 2.3-m with an equivalent isotropic radiated power of 31-dBm. The feasibility of the antenna-integrated HTS in estimating spinal cord and nerve injuries was demonstrated using a knee-jerk reflex test. When the distance between the transmitter's antenna and the antenna-integrated HTS was 0.5-m and the transmitted effective isotopically radiated power was 28.8-dBm, and a received power variation from −80.8 to −59.7-dBm was observed according to the leg movement.

INDEX TERMS Harmonic transponder sensor (HTS), knee-jerk reflex test, radar sensor, motion sensing.

I. INTRODUCTION

Recently, the use of radar sensors expanded into various fields, from typical automotive and military applications to contactless health monitoring applications [1], [2], [3]. However, it is difficult to detect electronic devices with relatively small scattering cross-sections using conventional radar sensors in noisy and reflective indoor environments such as inside buildings with many linear reflective structures. The limitations of radar sensors can be overcome with the use of harmonic radar sensors, which can easily detect small electronic signals in noisy and reflective indoor environments. Because the harmonic radar transmits fundamental signals and receives harmonic signals generated from nonlinear electronic targets, it is robust to clutter and jamming, obtaining a high signal-to-noise ratio in highly noisy and reflective indoor environments [4], [5].

A harmonic transponder sensor (HTS), which receives a fundamental signal and backscatters a harmonic signal, can be used with harmonic radars for various long-distance

The associate editor coordinating the review of this manuscript and approving it for publication was Mohamed Kheir.

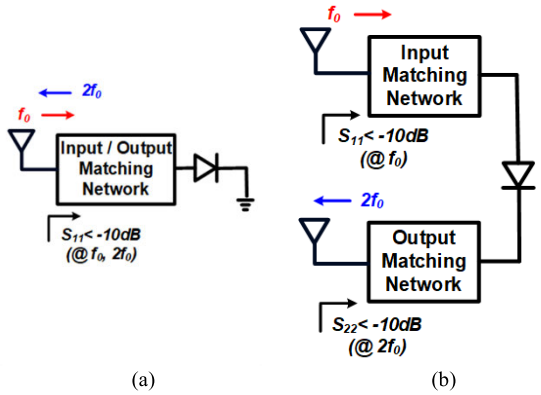

FIGURE 1. Architectural comparison of conventional HTSs: (a) reflection-type and (b) through-type.

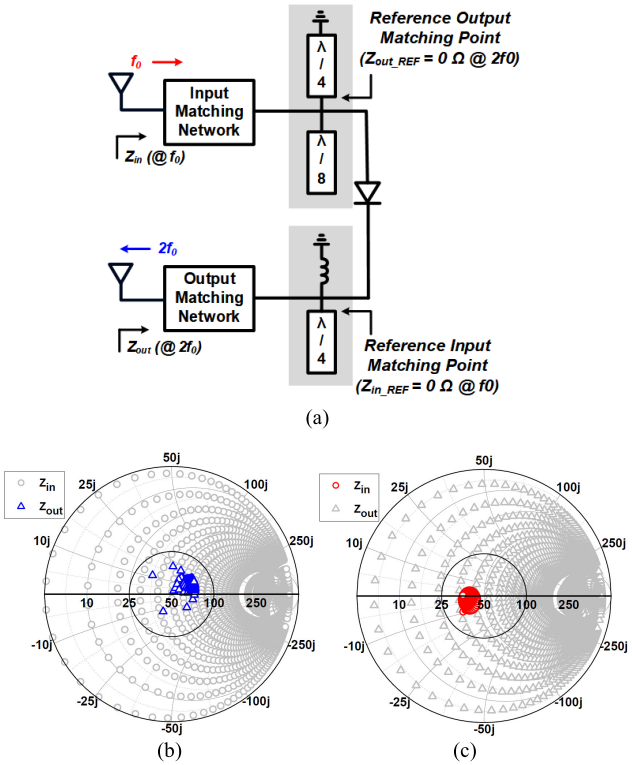

FIGURE 2. (a) Concept diagram of the proposed HTS. (b) Simulated output impedance of the proposed HTS with varying input impedance from short to open, and (c) simulated input impedance with varying output impedance from short to open.

sensing applications, including contactless health monitoring, RF wireless power transfer, security systems, and temperature sensing [6], [7], [8], [9], [10], [11], [12], [13], [14], [15], [16], [17], [18]. This is because harmonic radars can receive relatively higher harmonic powers from an HTS than those without an HTS. To extend the detection range of the HTS for various applications, a high conversion gain (CG) should be maintained over a wide input power and frequency range while minimizing the reflection of the fundamental signal.

As shown in Fig. 1, two types of conventional HTSs have been reported: reflection and through-type. The conventional reflection-type HTS, which has a single port that receives fundamental signals and transmits harmonic signals simultaneously, can be implemented in a small size with a dual-band matching network, as shown in Fig. 1(a). However, because the dual- band matching network matches the diode to the load at the fundamental and second harmonic frequencies, the fundamental signal reflected from the diode cannot be suppressed. The conventional through-type HTS can suppress the fundamental signal in the output matching network because the input and output matching networks can be separated at both ends of the diode, as shown in Fig. 1(b). However, the antenna impedance change caused by the attachment position of the conventional through-type HTS can affect its input and output impedances. Furthermore, the input and output matching network of the conventional through-type HTS must be optimized iteratively to match at the optimum impedance because the input and output impedances of the HTS affect each other.

In this paper, an HTS based on independent impedance control is introduced for motion sensing. The proposed through-type HTS comprises an independent impedance control matching network (IICMN) that suppresses the fundamental signal and minimizes the effect of the output (or input) impedance due to the impedance mismatch of the input (or output) caused by environmental changes near the sensor. The measured results of the implemented HTS showed that its CG of over −20 dB is maintained within a power range of −25–5 dBm at 3.1 GHz and a frequency range of 3.05–3.2 GHz at an input power of −13.7 dBm. The harmonic response of the proposed HTS was demonstrated at a distance of 0.3–2.3 m between a transceiver and the HTS. A knee-jerk reflex test was conducted with the antenna-integrated HTS in the indoor environment to verify the potential of the proposed HTS as a health monitoring sensor. When attached to a shin, the power received from the HTS varied by up to 20 dB, depending on the leg movement.

II. PROPOSED HTS WITH AN INDEPENDENT IMPEDANCE CONTROL MATCHING NETWORK

A. DESIGN ANALYSIS OF THE INDEPENDENT IMPEDANCE CONTROL MATCHING NETWORK

The HTS, which receives a fundamental wave signal and transmits a harmonic signal, is composed of an input matching stage at fundamental frequencies, a diode for harmonic generation using its nonlinearity, and an output matching stage at harmonic frequencies. For the HTS to function as a motion sensor, performance changes owing to the attachment location and environmental changes around the HTS should be minimized. However, antenna impedance changes can occur depending on the attachment position of the HTS, resulting in the deterioration of the harmonic output performance. Furthermore, it is difficult to match the input

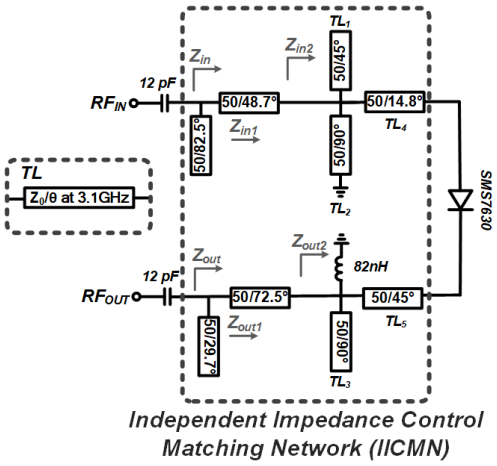

FIGURE 3. Schematic of the proposed HTS.

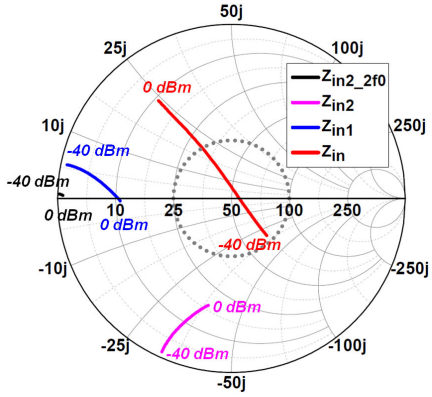

(a)

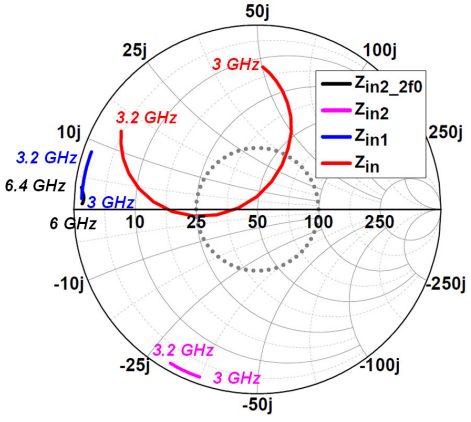

(b)

FIGURE 4. Simulated input impedance of the proposed HTS (a) with different input power levels at 3.1 and 6.2 GHz and (b) with different frequencies at an input power of −20 dBm.

and output impedances using conventional input and output matching networks because these values are coupled.

In this paper, an IICMN is proposed for independent impedance control of the HTS for input and output impedances at fundamental and second harmonic frequencies, respectively, to minimize impedance mismatch due to

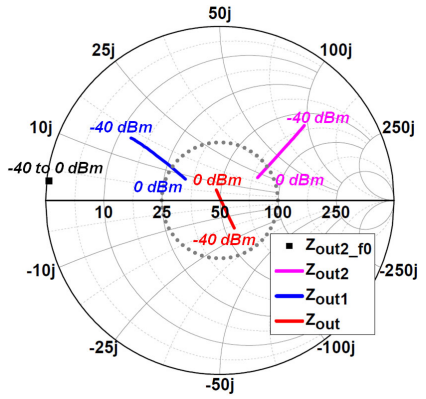

(a)

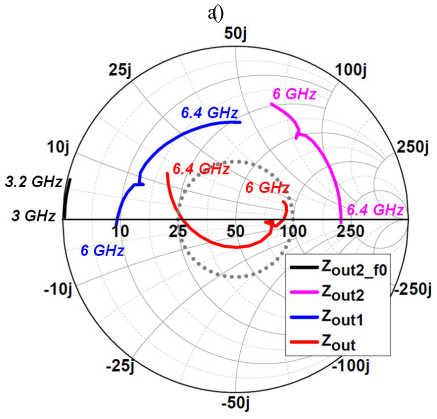

(b)

FIGURE 5. Simulated output impedance of the proposed HTS (a) with different input power levels at 3.1 GHz and 6.2 GHz and (b) with different frequencies at an input power at −20 dBm.

variation in the antenna impedance. A conceptual diagram of the IICMN adopted for HTS is shown in Fig. 2(a). The input stage of the IICMN is composed of a λ/4 short stub for the DC feed, a λ/8 open stub to obtain a short impedance value at second harmonic frequencies, and an L-shaped fundamental matching network. The output stage of the IICMN is composed of a λ/4 open stub with a short impedance value at fundamental frequencies, a shunt inductor for the DC feed, and an L-shaped second harmonic matching network.

When the input antenna impedance varies from short to open, as shown in Fig. 2(b), the output impedance Z_{out} of the HTS, which is in the VSWR = 2 circle, be insensitive to the variation of the input antenna impedance. Similarly, when the output antenna impedance is varied from short to open, as shown in Fig. 2(c), the input impedance Z_{in} of the HTS, which is in the VSWR = 2 circle, is insensitive to the variation in the output antenna impedance.

A schematic of the proposed HTS based on the IICMN is shown in Fig. 3. The proposed HTS consists of an input IICMN, a Schottky diode, and an output IICMN. The input and output IICMNs consist of an L-shaped matching network and T-shaped second harmonic and fundamental control network, respectively. In this design, the electrical lengths of TL_1 and TL_3 are fixed at λ/8 and λ/4 at 3.1 GHz, respectively,

TABLE 1. Comparison of recently reported harmonic transponders.

Ref.	Year	Type	Power range for CG > -15 dB (dB)	Peak CG.			Output freq. range for CG > -20 dB (GHz)	Size (λ_g^2)
				Freq. (GHz)	Input power (dBm)	CG (dB)		
This work	2023	Through	11	3.1	−13.7	−14.3	6.1–6.4	0.82 × 0.54
[16]	2022	Through	8[a]	2.5	0 [a]	−13 [a]	4.836–5.198	0.525 × 0.525
[17]	2022	Through	N/A	1.04	−10	−15.1	N/A	0.113 × 0.173
[12] [b]	2022	Reflect	27[a]	0.894	−20	−5	N/A	0.912 × 0.3
[14]	2020	Through	N/A	2.2	0	−15	4–6.4	N/A
[15]	2019	Through	N/A	3.5	−25	−17	N/A	0.48 × 0.48

a: graphically estimated, b: measured with antenna.

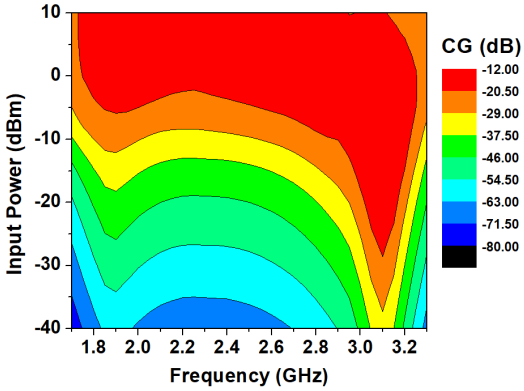

FIGURE 6. Simulated CG of the proposed HTS.

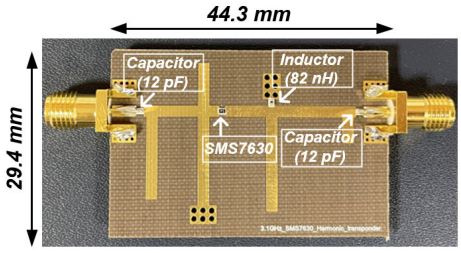

FIGURE 7. Photograph of the implemented HTS.

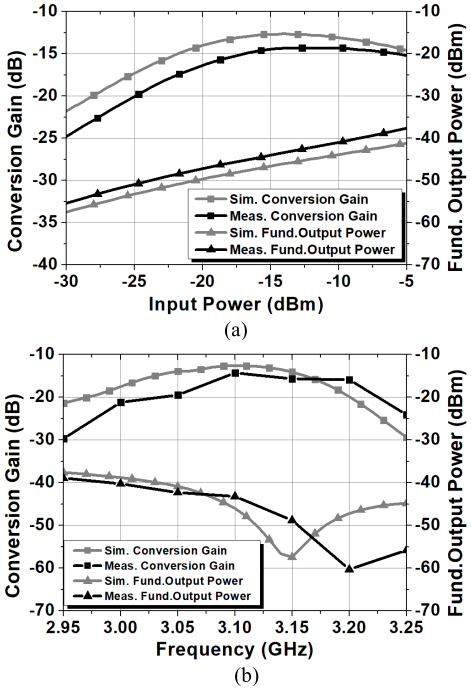

FIGURE 8. Simulated and measured results of CG and fundamental output power (a) at different input powers at 3.1 GHz and (b) at different operating frequencies at −13.7 dBm.

to control the input and output impedance independently. The width of TL_3 and the width and length of TL_5 are optimized to compensate for the negative imaginary part of the input impedance Z_{in2} at the fundamental frequencies before the input matching network. Subsequently, the L-shaped input matching network is optimized to move Z_{in2} within the VSWR = 2 circle in an input power range of −40 to −13.5 dBm at 3.1 GHz to achieve a high CG over a wide input power range, as shown in Fig. 4(a). Fig. 4(b) shows the input impedance according to the frequency at an input power of −20 dBm. The input impedance Z_{in} exists in the VSWR = 2 circle at 3.1 GHz.

The width of TL_1 and TL_2 and the width and length of TL_4 are also optimized to compensate for the negative imaginary part of the input impedance Z_{out2} at the second harmonic frequencies before the output matching network. The L-shaped output matching network is optimized to move Z_{out2} in the VSWR = 2 circle over a wide input power range of −40–0 dBm at 6.2 GHz, as shown in Fig. 5(a). Fig. 5(b) shows the output impedances of the HTS according to the frequency at an input power of −20 dBm, and Z_{out} is in the VSWR = 2 circle in the output frequency range of 6–6.3 GHz.

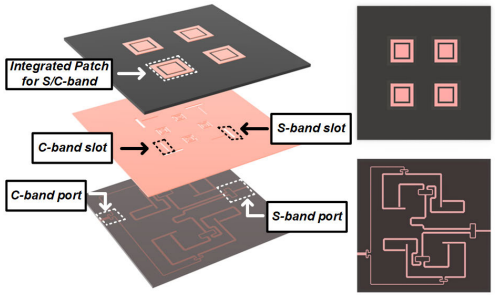

FIGURE 9. Overall geometry of the implemented S/C dual-band antenna for harmonic detection [19].

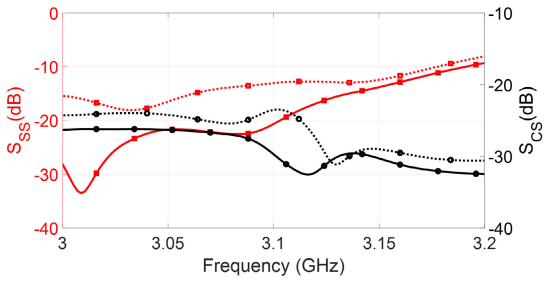

FIGURE 10. Simulated (dashed) and measured (solid) reflection coefficient S_{SS} and isolation S_{CS} of the proposed antenna at the S-band port.

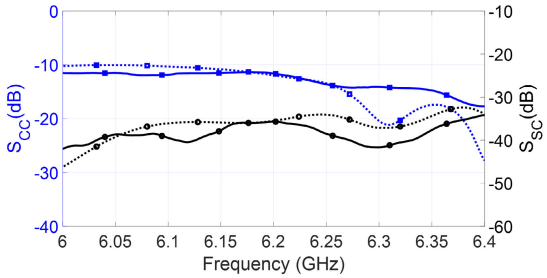

FIGURE 11. Simulated (dashed) and measured (solid) reflection coefficient S_{CC} and isolation S_{SC} of the proposed antenna at the C-band port.

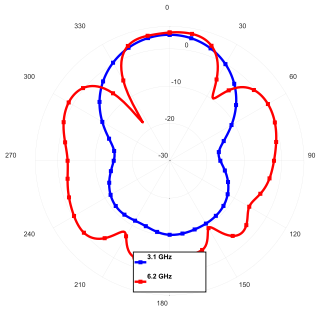

FIGURE 12. Simulated radiation patterns of the implemented S/C dual-band antenna at 3.1 (RHCP) and 6.2 GHz (LHCP).

Fig. 6 shows the simulated CG of the proposed HTS with varying input powers and frequencies. The CG is the difference between the second harmonic and fundamental signals. The simulation results showed a high CG in the frequency range that did not match to 50 Ω because a diode has a good nonlinear response at a high input power than at a low input power even when it does not match to 50 Ω. The proposed HTS had a peak CG of −12.6 dB at 3.1 GHz at an input power of −14 dBm. The CG of the proposed HTS was maintained over −20 dB within the frequency range of 1.8 to 3.2 GHz when the input power varied from −2 to 10 dBm.

B. IMPLEMENTATION AND MEASUREMENT RESULTS

The proposed HTS was fabricated on a Taconic TLC-32 substrate ($\varepsilon_r = 3.2$) with a thickness of 0.79 mm and total circuit size of 44.3 mm × 29.4 mm, as shown in Fig. 7. An SMS7630 diode was used in this design for a high CG at a low input power and high frequency [11]. An electromagnetic (EM) and circuit co-simulation was performed using the Keysight Advanced Design System (ADS) simulator. To measure the second harmonic output power of the implemented HTS, we generated the RF fundamental incident power using an N5182A signal generator, and the generated second harmonic signal was captured using an E440B spectrum analyzer.

Fig. 8(a) shows that the implemented HTS had a peak CG of −14.3 dB and output a fundamental power of −43.2 dBm at an input power of −13.7 dBm when the incident signal frequency was 3.1 GHz. It also achieved a CG of over −20 dB within the input frequency range of 3.05–3.2 GHz at an input power of −13.7 dBm, as shown in Fig. 7(b). Table 1 compares the performances of previously reported and proposed HTSs. The reflect type HTS in [12] was proposed to have high CG at low input power levels, but it can only operate at a single frequency. The through type HTSs in [14], [15], [16], and [17] have a compact size, making them suitable for various applications such as RFID, IoT and temperature sensing. However, the measured CG in [14], [15], and [17] is below −15 dB. In contrast, the proposed HTS achieves higher CG over a wider input power range. The performance of the proposed HTS was superior to that in [12] in terms of the operating frequency range.

III. HARMONIC SENSING TECHNOLOGY

A. IMPLEMENTED S/C DUAL-BAND ANTENNA

Fig. 9 shows the circularly polarized S/C dual-band antenna with a shared-aperture configuration that can be used for detecting nonlinear targets regardless of their orientation and polarization [19]. A 2.36 mm-thick Taconic TLC-32 substrate ($\varepsilon_r = 3.2$) was used for the top layer of the antenna, on which the integrated patch for the S/C-band was printed, A 0.762 mm-thick Rogers DiClad 88-IM laminate ($\varepsilon_r = 2.17$) was used for the bottom layer that housed the feeding networks for both channels. As depicted in Fig. 9, a rectangular complementary split ring resonator (RCSRR) on the ground plane prevented the transmitted S-band signals from interfering with the received C-band signals, increasing a port-to-port isolation.

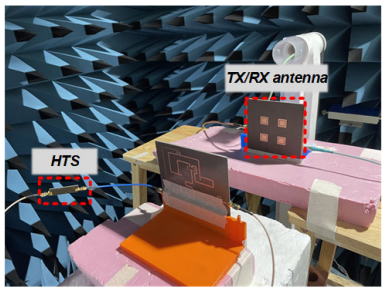

FIGURE 13. Setup for measuring the received second harmonic power with different EIRPs and distances.

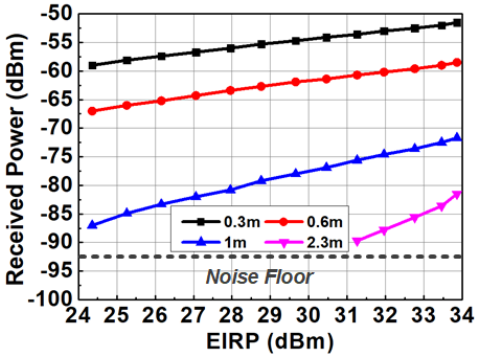

FIGURE 14. Measurement results of the received second harmonic power with varying EIRPs and sensing distances.

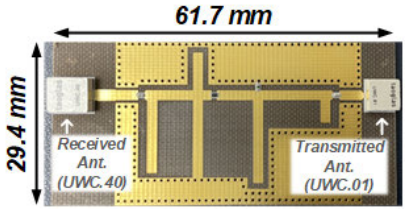

FIGURE 15. Photograph of the implemented antenna-integrated HTS.

Fig. 10 shows the simulated and measured reflection coefficient at S-band port (S_{SS}) and isolation between S- and C-band ports (S_{CS}). The measured S_{SS} is −20.5 dB at 3.1 GHz and S_{CS} exhibits a good isolation level below −20 dB at the same frequency. In Fig. 11, the simulated and measured reflection coefficients at C-band port (S_{CC}) are plotted, as well as the level of isolation between S- and C-band ports (S_{SC}). The measured S_{CC} is −11.8 dB at 6.2 GHz and S_{SC} exhibits a good isolation level below −20 dB at the corresponding frequency. The simulated radiation patterns in the S-band and C-band are plotted in Fig. 12. The maximum broadside gain was 3.74 dBi at 3.1 GHz and 4.75 dBi at 6.2 GHz.

B. NONLINEAR RESPONSE CHARACTERISTIC OF THE PROPOSED HTS

A harmonic detection test was conducted using a harmonic radar to verify the nonlinear response characteristics of the proposed HTS, as shown in Fig. 13. The transmitter of the harmonic radar was configured with an S/C dual-band antenna, harmonic suppressed C-band power amplifier [20], and signal generator. Considering the insertion loss of the coaxial line for the connection, the maximum effective isotopically radiated power (EIRP) of the transmitter was 34 dBm. The receiver of the harmonic radar was configured with a high-pass filter and a spectrum analyzer. As shown in Fig. 14, the received power of the harmonic radar was measured according to the EIRP within a sensing distance range of 0.3–2.3 m.

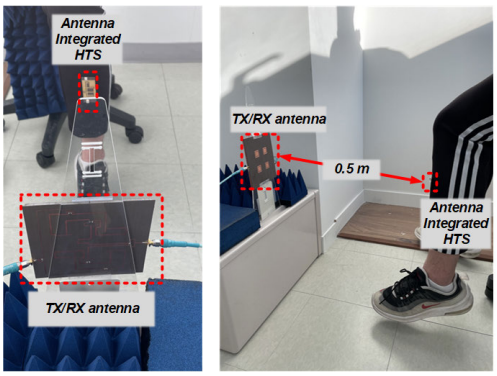

(a) (b)

FIGURE 16. Measurement setup for estimating spinal cord and nerve injury through a knee-jerk reflex (a) front view (b) side view.

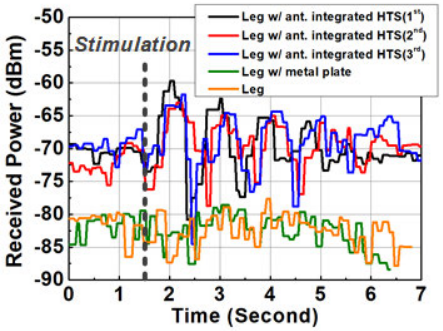

FIGURE 17. Measurement results of the received second harmonic power by shin movement at 28.8 dBm of EIRP at 0.5 m.

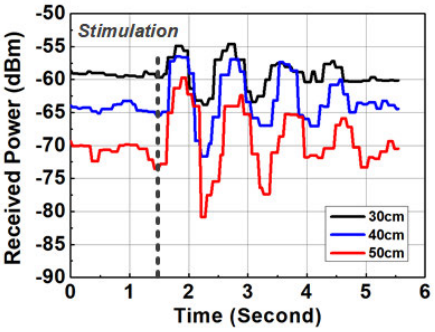

FIGURE 18. Measurement results of the received second harmonic power by shin movement at 28.8 dBm of EIRP with various distance.

The received power levels varied from −51.5 to −81.5 dBm within the distance of 0.3–2.3 m at an EIRP of 34 dBm.

C. ESTIMATION OF KNEE-JERK REFLEX BASED ON THE ANTENNA-INTEGRATED HTS

Knee-jerk reflex measurements, which are used to assess spinal cord and nerve injuries, were conducted to verify the feasibility of the proposed HTS as a motion sensor for health monitoring applications in a noisy and reflective indoor environment. A Taoglas UWC.40 chip antenna, which has a gain of 3.5 dBi at 3.1 GHz and size of 6 mm × 7 mm, is used as the linear polarized receiving antenna of the HTS [21]. A Taoglas UWC.01 chip antenna, which has a gain of 4.5 dBi at 6.2 GHz and size of 5.5 mm × 5.5 mm, is used as the linear polarized transmitting antenna of the HTS [22]. As shown in Fig. 15, the size of the implemented antenna-integrated HTS was 61.7 mm × 29.4 mm. The ground plane in the antenna-integrated HTS was added to meet the recommended ground size of the chip antennas, which is 26 mm × 20 mm. The transmitter and receiver were configured identically to the measurement setup used to determine the nonlinear response characteristic of the proposed HTS. A polarization loss of 3 dB occurs in each path since the TX/RX antenna and HTS antenna have circular and linear polarizations, respectively. The sensing distance between the TX/RX antenna and the antenna- integrated HTS was 0.5 m.

The maximum EIRP of the transmitter was 28.8 dBm.

Fig. 16 shows the setup for measuring knee-jerk reflex. The second harmonic power received from the antenna-integrated HTS attached to the shin was measured when the knee was stimulated. The harmonic signals reflected by shin movement without the antenna-integrated HTS and with a metal plate were also measured according to the transmitted harmonic signal to check whether a second harmonic signal occurred due to reflection by the shin movement. The received power oscillated according to the distance between the TX/RX antenna and HTS because the amplitude was changed by the shin movement.

As shown in Fig. 17, the measurement results indicated that the received harmonic power according to the movement of the shin due to knee stimulation ranged from −80 to −60 dBm. The knee-jerk reflex measurement based on the antenna-integrated HTS is robust in noisy and reflective indoor environments, as evidenced by the received second harmonic power from the shin without the antenna-integrated HTS and with a metal plate ranging from −78 to −88 dBm, which was close to the noise floor of −82.5 dBm. Fig. 18 also shows that the knee reflex test was well measured according to various distances from 30 to 50 cm in a noisy and reflective indoor environment.

In previous research on motion sensors [1], [2], [3], signal measurement using the Doppler effect required additional filtering and amplification to reprocess the signal when the received power was small or the received signal frequency was very low. According to the measurement results, the proposed HTS can easily acquire motion signals by measuring the received second harmonic power without requiring complex signal reprocessing in noisy and reflective indoor environments. In further research, an HTS that can modulate the second harmonic signal will be designed for identification and communication and experimentally demonstrated for multiple-target motion sensing. [17].

IV. CONCLUSION

This paper presents an HTS that can detect body movements such as knee-jerk reflexes, in noisy and reflective indoor environments. An IICMN is adopted on each side of the diode in the HTS to independently control the input and output impedances and match them to the source and load impedances within the wide input power and frequency ranges, irrespective of the change in antenna impedance according to the sensor attachment position. The proposed HTS achieves a CG of over −20 dB within the input power range of −25–5 dBm at 3.1 GHz and the frequency range of 3.05–3.2 GHz at an input power of −13.7 dBm.

The HTS was also implemented with a dual-band antenna to evaluate the nonlinear reflection characteristics with respect to the EIRP of the transmitter and distance between the transmitter and HTS. The received power reflected from the HTS ranged from −51.5 to −81.5 dBm within the distance range of 0.3–2.3 m at 34 dBm of EIRP and from −87 to −71.7 dBm within the EIRP range of 24.4–33.9 dBm at a distance of 1.0 m. The feasibility of the proposed antenna-integrated HTS as a wireless motion sensor in a noisy and reflective indoor environment was investigated using knee-jerk reflex tests by attaching the antenna-integrated HTS to the shin of a participant; a reflected power variation of over 20 dB was detected according to the movement of the leg.

ACKNOWLEDGMENT

The EDA tool was supported by the IC Design Education Center (IDEC), South Korea.

REFERENCES

[1] M. Kebe, R. Gadhafi, B. Mohammad, M. Sanduleanu, H. Saleh, and M. Al-Qutayri, "Human vital signs detection methods and potential using radars: A review," *Sensors*, vol. 20, no. 5, p. 1454, Mar. 2020.

[2] J.-H. Park, Y.-J. Jeong, G.-E. Lee, J.-T. Oh, and J.-R. Yang, "915-MHz continuous-wave Doppler radar sensor for detection of vital signs," *Electronics*, vol. 8, no. 5, p. 561, May 2019.

[3] E. Hyun, Y. S. Jin, J. H. Park, and J. R. Yang, "Machine learning-based human recognition scheme using a Doppler radar sensor for in-vehicle applications," *Sensors*, vol. 20, no. 21, p. 6202, Oct. 2020.

[4] R. Hstger, "Harmonic radar systems for near-ground in-foliage nonlinear scatterers," *IEEE Trans. Aerosp. Electron. Syst.*, vol. AES-12, no. 2, pp. 230–245, Mar. 1976.

[5] G. J. Mazzaro, A. F. Martone, K. I. Ranney, and R. M. Narayanan, "Nonlinear radar for finding RF electronics: System design and recent advancements," *IEEE Trans. Microw. Theory Techn.*, vol. 65, no. 5, pp. 1716–1726, May 2017.

[6] L. Zhu, T. D. Hà, Y.-H. Chen, H. Huang, and P.-Y. Chen, "A passive smart face mask for wireless cough monitoring: A harmonic detection scheme with clutter rejection," *IEEE Trans. Biomed. Circuits Syst.*, vol. 16, no. 1, pp. 129–137, Feb. 2022.

[7] M.-L. Hsu, T.-H. Liu, T.-C. Yang, H.-C. Jhan, H. Wang, F.-R. Chang, K.-Y. Lin, E.-C. Yang, and Z.-M. Tsai, "Bee searching radar with high transmit-receive isolation using pulse pseudorandom code," *IEEE Trans. Microw. Theory Techn.*, vol. 64, no. 12, pp. 4324–4335, Dec. 2016.

[8] A. Mishra, W. McDonnell, J. Wang, D. Rodriguez, and C. Li, "Intermodulation-based nonlinear smart health sensing of human vital signs and location," *IEEE Access*, vol. 7, pp. 158284–158295, 2019.
[9] X. Hui, T. B. Conroy, and E. C. Kan, "Near-field coherent sensing of vibration with harmonic analysis and balance signal injection," *IEEE Trans. Microw. Theory Techn.*, vol. 69, no. 3, pp. 1906–1916, Mar. 2021.
[10] R. Raju, G. E. Bridges, and S. Bhadra, "Wireless passive sensors for food quality monitoring: Improving the safety of food products," *IEEE Antennas Propag. Mag.*, vol. 62, no. 5, pp. 76–89, Oct. 2020.
[11] X. Gu, P. Burasa, S. Hemour, and K. Wu, "Recycling ambient RF energy: Far-field wireless power transfer and harmonic backscattering," *IEEE Microw. Mag.*, vol. 22, no. 9, pp. 60–78, Sep. 2021.
[12] M. Polivka, V. Hubata-Vacek, and M. Svanda, "Harmonic balance/full-wave analysis of wearable harmonic transponder for IoT applications," *IEEE Trans. Antennas Propag.*, vol. 70, no. 2, pp. 977–987, Feb. 2022.
[13] A. Lavrenko, B. Litchfield, G. Woodward, and S. Pawson, "Design and evaluation of a compact harmonic transponder for insect tracking," *IEEE Microw. Wireless Compon. Lett.*, vol. 30, no. 4, pp. 445–448, Apr. 2020.
[14] L. Zhu, H. Huang, M. M. Cheng, and P.-Y. Chen, "Compact, flexible harmonic transponder sensor with multiplexed sensing capabilities for rapid, contactless microfluidic diagnosis," *IEEE Trans. Microw. Theory Techn.*, vol. 68, no. 11, pp. 4846–4854, Nov. 2020.
[15] X. Gu, N. N. Srinaga, L. Guo, S. Hemour, and K. Wu, "Diplexer-based fully passive harmonic transponder for sub-6-GHz 5G-compatible IoT applications," *IEEE Trans. Microw. Theory Techn.*, vol. 67, no. 5, pp. 1675–1687, May 2019.
[16] R. Raju and G. E. Bridges, "A compact wireless passive harmonic sensor for packaged food quality monitoring," *IEEE Trans. Microw. Theory Techn.*, vol. 70, no. 4, pp. 2389–2397, Apr. 2022.
[17] V. Palazzi, L. Roselli, M. M. Tentzeris, P. Mezzanotte, and F. Alimenti, "Energy-efficient harmonic transponder based on on-off keying modulation for both identification and sensing," *Sensors*, vol. 22, no. 2, p. 620, Jan. 2022.
[18] T. M. Silveira, P. Pinho, and N. B. Carvalho, "Harmonic RFID temperature sensor design for harsh environments," *IEEE Microw. Wireless Compon. Lett.*, vol. 32, no. 10, pp. 1239–1242, Oct. 2022.
[19] S. Oh, H. S. Park, J. Oh, and S. K. Hong, "Circularly polarized S/C dual-band antenna for nonlinear detection," *IEEE Antennas Wireless Propag. Lett.*, vol. 21, no. 7, pp. 1467–1471, Jul. 2022.
[20] J. Kim, S. K. Hong, and J. Oh, "Highly efficient power amplifier based on harmonic-controlled matching network," *IEEE Microw. Wireless Technol. Lett.*, vol. 33, no. 1, pp. 43–46, Jan. 2023.
[21] Taoglas. *UWC.40 Datasheet*. Accessed: May 5, 2022. [Online]. Available: https://www.taoglas.com/datasheets/UWC.40.pdf
[22] Taoglas. *UWC.01 Datasheet*. Accessed: Jun. 8, 2022. [Online]. Available: https://www.taoglas.com/datasheets/UWC.01.pdf

JISU KIM (Student Member, IEEE) received the B.S. degree from the Department of Robotics Engineering, Yeungnam University, Gyeongsan, South Korea, in 2021. She is currently pursuing the integrated M.S. and Ph.D. degrees in electronic engineering from Soongsil University, Seoul, South Korea. Her research interests include wireless power transfer technology and radar systems.

SOOYOUNG OH (Student Member, IEEE) received the B.S. degree in electronic engineering from Soongsil University, Seoul, South Korea, in 2021, where he is currently pursuing the combined M.S. and Ph.D. degrees in electronic engineering. His research interests include mm-wave devices, nonlinear radars, radar signal processing, and antennas for nonlinear detection.

BITCHAN KIM (Student Member, IEEE) received the B.S. degree in electronic engineering from Soongsil University, Seoul, South Korea, in 2022, and where he is currently pursuing the M.S. degree in electronic engineering. His main research interest includes power amplifiers for multi-band harmonic-radar systems.

JUNTAEK OH (Member, IEEE) received the B.S., M.S., and Ph.D. degrees in electronics and electrical engineering from the Korea Advanced Institute of Science and Technology (KAIST), Daejeon, South Korea, in 2010, 2012, and 2016, respectively.

From 2016 to 2018, he was with the Advanced Medical Device Research Division, Korea Electrotechnology Research Institute (KERI), Ansan, South Korea. From 2018 to 2020, he was an Assistant Professor with the Department of Robotics Engineering, Yeungnam University, Gyeongsan, South Korea. Since 2020, he has been with the School of Electronic Engineering, Soongsil University, where he is currently an Associate Professor. His main research interests include analog/RF/mmW CMOS ICs and radar systems.